

# Constraints on Cosmological Models from Quasars Calibrated with Type Ia Supernova by a Gaussian Process

Haixiang Zhang<sup>1</sup>, Yang Liu<sup>\* 1</sup>, Hongwei Yu<sup>1,5, †</sup>, Xiaodong Nong<sup>2,3,4</sup>, Nan Liang<sup>‡ 2,3,4</sup> and Puxun Wu<sup>1,5 §</sup>

<sup>1</sup>Department of Physics and Synergistic Innovation Center for Quantum Effects and Applications, Hunan Normal University, Changsha, Hunan 410081, China

<sup>2</sup>Key Laboratory of Information and Computing Science Guizhou Province, Guizhou Normal University, Guiyang, Guizhou 550025, China

<sup>3</sup>School of Cyber Science and Technology, Guizhou Normal University, Guiyang, Guizhou 550025, China

<sup>4</sup>Joint Center for FAST Sciences Guizhou Normal University Node, Guiyang, Guizhou 550025, China

<sup>5</sup>Institute of Interdisciplinary Studies, Hunan Normal University, Changsha, Hunan 410081, China

25 April 2024

## ABSTRACT

In this paper, we use quasars calibrated from type Ia supernova (SN Ia) to constrain cosmological models. We consider three different X-ray luminosity ( $L_X$ ) - ultraviolet luminosity ( $L_{UV}$ ) relations of quasars, i.e., the standard  $L_X$ - $L_{UV}$  relation and two redshift-evolutionary relations (Type I and Type II) respectively constructed from copula and considering a redshift correction to the luminosity of quasars. Only in the case of the Type I relation, quasars can always provide effective constraints on the  $\Lambda$ CDM model. Furthermore, we show that, when the observational Hubble data (OHD) are added, the constraints on the absolute magnitude  $M$  of SN Ia and the Hubble constant  $H_0$  can be obtained. In the  $\Lambda$ CDM model, the OHD measurements plus quasars with the Type I relation yields  $M = -19.321^{+0.085}_{-0.076}$ , which is in good agreement with the measurement from SH0ES ( $M = -19.253 \pm 0.027$ ), and  $H_0 = 70.80 \pm 3.6 \text{ km s}^{-1} \text{ Mpc}^{-1}$ , falling between the measurements from SH0ES and the Planck cosmic microwave background radiation data.

**Key words:** Quasars: general - (*cosmology:*) dark energy - cosmology: observations

## 1 INTRODUCTION

The  $\Lambda$ CDM (cosmological constant  $\Lambda$  plus cold dark matter) model is the simplest cosmological model to explain the accelerating cosmic expansion. Although consistent with many observations (Perlmutter et al. 1999; Riess et al. 1998; Alam et al. 2021; Brout et al. 2022), it still suffers the Hubble tension (Riess 2020; Di Valentino et al. 2021; Perivolaropoulos et al. 2022; Dainotti et al. 2021, 2022a; Liu, Yu & Wu 2023), which refers to the more than  $5\sigma$  disagreement between the constraints on the Hubble constant  $H_0$  from the nearby type Ia supernova (SN Ia) and the cosmic microwave background (CMB) radiation data, respectively. Using the latest SN Ia measurements, Riess et al. (2022) obtain  $H_0 = 73.04 \pm 1.04 \text{ km s}^{-1} \text{ Mpc}^{-1}$  in a model-independent manner, while the CMB data from the Planck 2018 survey yield  $H_0 = 67.36 \pm 0.54 \text{ km s}^{-1} \text{ Mpc}^{-1}$  (Planck Collaboration 2020) in the framework of the  $\Lambda$ CDM model. Many other observational data have been utilized to search the possible origins of the  $H_0$  tension, but a satisfactory explanation remains elusive. Since the redshift range of commonly used observations, including SN Ia (Scolnic et al. 2022), observational Hubble parameter data (OHD) (Moresco et al. 2020), baryon acoustic oscillations (Eisenstein et al. 2005), and strong gravitational lenses (Suyu et al. 2010, 2013), reaches only about  $z \sim 2$ , while the CMB data is near  $z \sim 1100$ , cosmological

data in the mid-redshift region ( $2 \lesssim z \lesssim 1100$ ) might offer important insights into the origins of the Hubble tension.

Quasars (quasi-stellar objects) are the extremely luminous and persistent sources of light found in the universe, which can be detected at  $z > 7$  (Mortlock et al. 2011; Bañados et al. 2017; Wang et al. 2021). To use quasars as the standard candles in cosmology, the luminosity relation of quasars needs to be constructed. In this regard, an empirical non-linear relation between the ultraviolet (UV) luminosity and the X-ray luminosity ( $L_X$ - $L_{UV}$ ) has been proposed in (Tanenbaum et al. 1979; Zamorani et al. 1981; Avni & Tanenbaum 1986; Risaliti & Lusso 2015), and it has been widely applied to investigate the high-redshift universe using quasars (Risaliti & Lusso 2015, 2019; Lusso & Risaliti 2016, 2017; Lusso et al. 2019, 2020; Velten & Gomes 2020; Khadka & Ratra 2020a,b, 2021; Khadka et al. 2023; Wei & Melia 2020; Li et al. 2021, 2024; Hu & Wang 2022a; Bargiacchi et al. 2022; Dainotti et al. 2023a). Recently, Khadka & Ratra (2020a) showed some evidences of redshift evolution of the X-ray and UV relation. By considering a power-law redshift correction  $((1+z)^k)$  to the quasar luminosity, Dainotti et al. (2022b) obtained a three-dimensional and redshift-evolutionary version of the  $L_X$ - $L_{UV}$  relation. In (Dainotti et al. 2022b), the coefficient of the redshift correction term is determined by using the Efron-Petrosian (EP) method (Efron & Petrosian 1992). This coefficient will be treated as a free parameter in the following analysis. Wang et al. (2022) introduced an improved three-dimensional  $L_X$ - $L_{UV}$  relation with a redshift-dependent term given by a powerful statistical tool called

\* Co-first author

† hwyu@hunnu.edu.cn

‡ liangn@bnu.edu.cn

§ pxwu@hunnu.edu.cn

copula<sup>1</sup>. The increased reliability of the  $L_X$ - $L_{UV}$  relations as a cosmological tool has been established in (Wang et al. 2022, 2024; Dainotti et al. 2022b; Lenart et al. 2023)

Similar to the Gamma-ray burst (GRB) cosmology, the quasar cosmology also suffers the so-called *circularity problem* since a fiducial cosmological model is usually assumed to calibrate the empirical relation when quasars are used to constrain the cosmological models. Inspired by the idea of distance ladder with the Cepheids and SN Ia, the *low-redshift calibration* has been proposed to calibrate the GRB relations from SN Ia to build the Hubble diagram of GRB (Liang et al. 2008, 2010, 2011; Kodama et al. 2008; Capozziello & Izzo 2008; Wei & Zhang 2009; Wei 2010; Liu & Wei 2015; Wang et al. 2016; Demianski et al. 2017; Liu et al. 2022b; Liang et al. 2022; Li et al. 2024; Mu et al. 2023; Xie et al. 2023). In addition, the simultaneous fitting or global fitting method has also been established to avoid the *circularity problem* in the GRB cosmology (Ghirlanda et al. 2004; Li et al. 2008; Dainotti et al. 2023b; Cao & Ratra 2024). Here, we want to apply the low-redshift calibration method in the quasar cosmology and calibrate the luminosity relations of quasars by using SN Ia.<sup>2</sup> To achieve the luminosity distance at the redshift of quasars from SN Ia, we need to employ a cosmological model-independent method to reconstruct the Hubble diagram of SN Ia. In this regard, let us note that the Gaussian process (GP) is a fully Bayesian statistical method used for reconstructing the Hubble diagram from existing data and predicting unknown data (Seikel et al. 2012a), which can effectively reduce errors in the reconstructed results. In recent years, the GP method has found extensive applications in the fields of cosmology and astrophysics (Seikel et al. 2012b; Busti et al. 2014; Yu & Wang 2016; Lin et al. 2018; Wei 2018; Yu et al. 2018; Pan et al. 2020; Hu & Wang 2022b).

Thus, in this paper, the GP method will be used to reconstruct the Hubble diagram of the 1590 Pantheon+ SN Ia data points, which are obtained by removing the data in the redshift region of  $z < 0.01$  from 1701 SN light curves of 1550 spectroscopically confirmed SN Ia with the maximum redshift being about  $z \sim 2.3$  (Scolnic et al. 2022), and then the luminosity distances of low-redshift quasars, which are the subset of the dataset comprising 2421 X-ray and UV flux measurements of quasars (Lusso et al. 2020), can be derived from the SN Ia Hubble diagram. From an initial dataset of 21,785 data points, a total of 2,421 quasars have been selected. These quasars originate from seven different samples, observed using instruments such as *Chandra* and *XMM-Newton*. Quasars displaying UV reddening, significant host-galaxy contamination in the near-infrared, or poor photometry data were excluded. Additionally, adjustments for Eddington bias were considered. Following these corrections, Lusso et al. (2020) compiled the final, refined sample of 2,421 quasars, covering a redshift range from 0.009 to 7.52. It is important to note that no  $K$ -correction was applied to the quasars (Bloom et al. 2001; Lusso et al. 2020). These low-redshift quasars can be used to determine the coefficients in different  $L_X$ - $L_{UV}$  relations. Extrapolating the results to the high-redshift quasars, we can obtain the luminosity distances of all quasars model-independently, and use these distances to constrain

the cosmological models. Since the quasar sample only cannot give constraints on the absolute magnitude ( $M$ ) of SN Ia and the Hubble constant ( $H_0$ ) simultaneously, we also add 32 OHD measurements obtained by the cosmic chronometers method (Moresco et al. 2020), which relate to the evolution of differential ages of passive galaxies at different redshifts (Jimenez & Loeb 2002), to obtain constraints on  $M$  and  $H_0$ .

The rest of this paper is organized as follow. In Section 2, we respectively calibrate, by using the low-redshift calibration method, three different  $L_X$ - $L_{UV}$  relations from SN Ia: the standard relation and two redshift-evolutionary relations (Type I and Type II) constructed from copula and considering a redshift correction to the luminosity of quasars. The constraints on different cosmological models from quasars and OHD are given in Section 3. Section 4 shows the discussion on results. Conclusions are summarized in Section 5.

## 2 CALIBRATING THE $L_X$ - $L_{UV}$ RELATIONS FROM SN IA

The standard  $L_X$ - $L_{UV}$  relation, which is a non-linear relation between the X-ray luminosity ( $L_X$ ) and the UV luminosity ( $L_{UV}$ ) of quasars (Tananbaum et al. 1979; Zamorani et al. 1981; Avni & Tananbaum 1986; Risaliti & Lusso 2015), takes the form

$$\log(L_X) = \beta + \gamma \log(L_{UV}). \quad (1)$$

Here  $\beta$  and  $\gamma$  are two coefficients, and “log” denotes the logarithm to the base 10. Expressing the luminosity in terms of the flux, one can obtain

$$\begin{aligned} \log(F_X) &= 2(\gamma - 1) \log(d_L) + \beta + (\gamma - 1) \log(4\pi) \\ &+ \gamma \log(F_{UV}). \end{aligned} \quad (2)$$

Here  $F_X = \frac{L_X}{4\pi d_L^2}$  and  $F_{UV} = \frac{L_{UV}}{4\pi d_L^2}$  are the observed flux of X-ray and UV, respectively, and  $d_L$  is the luminosity distance, which contains the information of cosmological models.

Recently, the standard  $L_X$ - $L_{UV}$  relation has been generalized to contain possible redshift-evolutionary effects:

$$\begin{aligned} \log(F_X) &= 2(\gamma - 1) \log(d_L) + \beta + (\gamma - 1) \log(4\pi) \\ &+ \gamma \log(F_{UV}) + \alpha \ln(\bar{\alpha} + z). \end{aligned} \quad (3)$$

Here  $\alpha$  is a coefficient, and  $\alpha \neq 0$  represents that the relation evolves with redshift. The constant  $\bar{\alpha}$  equals to 1 or 5. When  $\bar{\alpha} = 5$ , the relation given in Eq. (3), which is named the Type I relation in this paper, corresponds to that constructed by using the copula function (Wang et al. 2022). If  $\bar{\alpha} = 1$ , the corresponding relation is called the Type II relation, and is obtained by assuming that the luminosity of quasars is corrected via a redshift-dependent function  $(1+z)^k$  (Dainotti et al. 2015, 2022b).

To apply quasars in cosmology, we need to obtain their luminosity distances from the observables of quasars by using the relations shown in Eqs. (2, 3). Apparently, the values of the coefficients ( $\alpha$ ,  $\beta$ ,  $\gamma$ ) need to be determined first. Here, we adopt the idea of distance ladder and use the SN Ia data to calibrate the  $L_X$ - $L_{UV}$  relations. Since the data points of SN Ia concentrate in the low-redshift ( $z \leq 1.4$ ) region, the SN Ia data from the latest Pantheon+ sample at  $z \leq 1.4$  (Scolnic et al. 2022) are utilized to determine  $\alpha$ ,  $\beta$  and  $\gamma$ . To avoid the effect of cosmological models on the calibration, we use the GP method (Seikel et al. 2012a) to construct the smooth curve of the apparent magnitude ( $m$ )-redshift relation of SN Ia. GP is a generalization of Gaussian distribution, which refers to the distribution of random variables, and describes the distribution over functions.

<sup>1</sup> Copula is a powerful tool developed in modern statistics to describe the correlation between multivariate random variables (Nelsen 2007) and it has been used to construct the redshift-evolutionary relation of Gamma-ray bursts (Liu et al. 2022a,b).

<sup>2</sup> As demonstrated in (Wang et al. 2022; Lenart et al. 2023), it has been established that certain cosmological parameters, such as  $\Omega_{m0}$ , are linearly independent of the correction coefficients. Hence, there is no impediment to constraining these parameters without calibration. However, calibration can significantly improve the precision of cosmological parameter estimation.

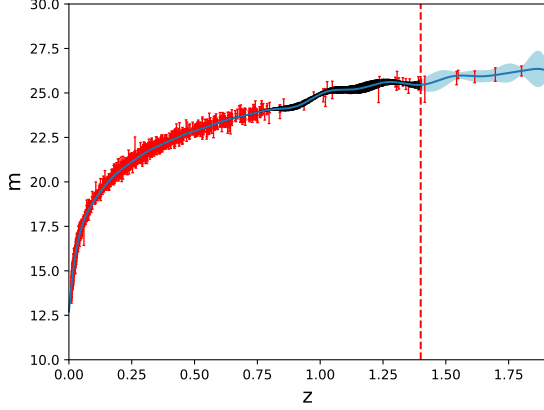


**Figure 1.** The blue curves depict the reconstructed function with  $1\sigma$  uncertainty from the SN Ia data (red dots) through Gaussian process. The red dashed line represents  $z = 1.4$ .

With the GP method, the smooth functions from a set of discrete data points can be constructed (Seikel et al. 2012a). Here we use an infinitely differentiable squared exponential covariance function to reconstruct the smooth functions of the apparent magnitude of SN Ia. The covariance function is given by:

$$k(z, \tilde{z}) = \sigma_f^2 \exp \left[ -\frac{(z - \tilde{z})^2}{2l^2} \right], \quad (4)$$

where the hyperparameters  $\sigma_f$  and  $l$  are optimized by maximizing the marginal likelihood<sup>3</sup>. When the Pantheon+ sample (Scolnic et al. 2022) is used, we exclude those data whose redshifts are less than 0.01 since the nearby SN Ia sample may be impacted by the peculiar velocities (Brout et al. 2022). The reconstructed  $m$ - $z$  relation with an uncertainty of  $1\sigma$  by using the GP is shown in Fig. 1. This figure indicates that the reconstructed result is well consistent with the data distribution.

The distance module  $\mu$  of SN Ia is related to the luminosity distance ( $d_L$ ) and the absolute magnitude ( $M$ ) through

$$\mu = m - M = 5 \log \left( \frac{d_L}{\text{Mpc}} \right) + 25. \quad (5)$$

Thus, the luminosity distance of quasars that fall in the redshift under  $z = 1.4$  may be obtained from the reconstructed  $m(z)$  after the value of  $M$  is determined. However, the value of  $M$  cannot be directly obtained using only the SN Ia sample and thus  $M$  is treated as a free parameter. Substituting Eq. (5) into the  $L_X$ - $L_{UV}$  relations, one can obtain

$$\log(F_X) = 2(\gamma - 1) \frac{m - M - 25}{5} + \beta + (\gamma - 1) \log(4\pi) + \gamma \log(F_{UV}) + \alpha \ln(\bar{\alpha} + z), \quad (6)$$

which shows that there is a strong degeneracy between the absolute magnitude  $M$  and the coefficient  $\beta$ . Thus, we cannot constrain the values of  $M$  and  $\beta$  simultaneously by using the observational data. To address this issue without assuming any prior values of  $M$ , we

introduce a new coefficient:  $\beta' = -2(\gamma - 1) \left( \frac{M}{5} + 5 \right) + \beta + (\gamma - 1) \log(4\pi)$ . Then, the relation Eq. (6) is reduced to

$$\log(F_X) = 2(\gamma - 1) \frac{m}{5} + \beta' + \gamma \log(F_{UV}) + \alpha \ln(\bar{\alpha} + z). \quad (7)$$

Using the apparent magnitude of SN Ia reconstructed at a redshift of quasars and the observed  $\log(F_{UV})_{\text{obs}}$  at this redshift, we can obtain  $\log(F_X)_{\text{re}}$  from Eq. (7). Comparing this  $\log(F_X)_{\text{re}}$  with the observed X-ray flux of quasars can give the values of  $\alpha$ ,  $\beta'$  and  $\gamma$  by maximizing the D'Agostinis likelihood function (D'Agostini 2005):

$$\mathcal{L}(\delta, \theta) = \prod_{i=1}^N \frac{1}{\sqrt{2\pi(\sigma_i^2 + \delta^2)}} \times \exp \left\{ -\frac{[\log(F_X)_{\text{obs},i} - \log(F_X)_{\text{re}}(\log(F_{UV})_{\text{obs},i}; \theta)]^2}{2(\sigma_i^2 + \delta^2)} \right\}, \quad (8)$$

where  $\delta$  is the intrinsic dispersion,  $\theta \equiv \{\alpha, \beta', \gamma\}$ , and  $\sigma_i^2 = \sigma_{\log(F_X)_{\text{obs},i}}^2 + \gamma^2 \sigma_{\log(F_{UV})_{\text{obs},i}}^2 + \left( \frac{2\gamma-2}{5} \right)^2 \sigma_m^2$  with  $\sigma_{\log(F_X)_{\text{obs},i}}$ ,  $\sigma_{\log(F_{UV})_{\text{obs},i}}$ , and  $\sigma_m$  being the uncertainties of  $\log(F_X)_{\text{obs},i}$ ,  $\log(F_{UV})_{\text{obs},i}$ , and the reconstructed  $m$ , respectively. In Eq. (8), number  $N = 1326$  is the number of quasars in the low-redshift ( $z \leq 1.4$ ) region. To find the maximum likelihood, we utilize the Python package *emcee* (Foreman-Mackey et al. 2013), which bases on the Metropolis-Hastings algorithm and implements the Markov Chain Monte Carlo (MCMC) numerical fitting method. The calibrated results for the coefficients in various  $L_X$ - $L_{UV}$  relations are presented in Tab. 1 and Fig. 2. Obviously, only the value of  $\delta$  is almost independent of the relations. The values of  $\gamma$  are almost the same in the Type I and II relations, but they deviate from that in the standard  $L_X$ - $L_{UV}$  relation. The Type I and standard relations give almost the same value of  $\beta'$ , which is smaller than the one in the Type II relation. The Type I and II relations give different values of  $\alpha$ , but both of them deviate from zero at more than  $3\sigma$ , which indicates that the observations seem to support the redshift-evolutionary relations.

To investigate the effect of different redshift borders, we also consider quasars in two different redshift regions ( $z \leq 1$  and  $z \leq 1.8$ ). The results are shown in Tab. 2. Comparing Tab. 1 with Tab. 2, we find that the relation coefficients and the intrinsic dispersions across these redshift regions vary slightly but remain consistent within a  $1\sigma$  CL. Thus, the choice of redshift borders exerts a negligible effect on the calibration of the luminosity relations. In the following analyses, we will use the results from quasars with  $z \leq 1.4$ .

To further check whether there exist selection biases and redshift evolution in quasar data (Singal et al. 2022, 2013, 2019), we follow the process given in (Dainotti et al. 2015, 2022b) and use the EP method (Efron & Petrosian 1992) to calculate the value of  $k$  parameter which is introduced to correct the luminosity via  $L_{\text{corrected}} = L_{\text{observed}} / (\bar{\alpha} + z)^k$  in Type I and II relations, and the corresponding value of  $\alpha$ . If the obtained value of  $\alpha$  is consistent with that from the low-redshift calibration, then the results presented in Table 1 are not influenced by selection biases or redshift evolution in quasars. When the correction to the luminosity is considered, we need to replace  $L_X$  and  $L_{UV}$  with  $L_X / (\bar{\alpha} + z)^{k_X}$  and  $L_{UV} / (\bar{\alpha} + z)^{k_{UV}}$  in Eq. (1). Then, we obtain the following simple relation between  $\alpha$  and  $k_X$  and  $k_{UV}$ :

$$\alpha = \frac{k_X - \gamma k_{UV}}{\ln 10}. \quad (9)$$

Clearly, the value of  $\alpha$  can be inferred from the values of  $k_X$  and  $k_{UV}$  when  $\gamma$  is known. The values of  $k_X$  and  $k_{UV}$  can be obtained by using the EP method, which is given in a publicly available Mathematica code: *Selection biases and redshift evolu-*

<sup>3</sup> In this work, we use the public PYTHON package **GaPP** to reconstruct the apparent magnitude ( $m$ )-redshift relation of SN Ia sample in low-redshift ( $z < 1.4$ ) region. This code is available at <https://github.com/astrobenjaly/GaPP>.

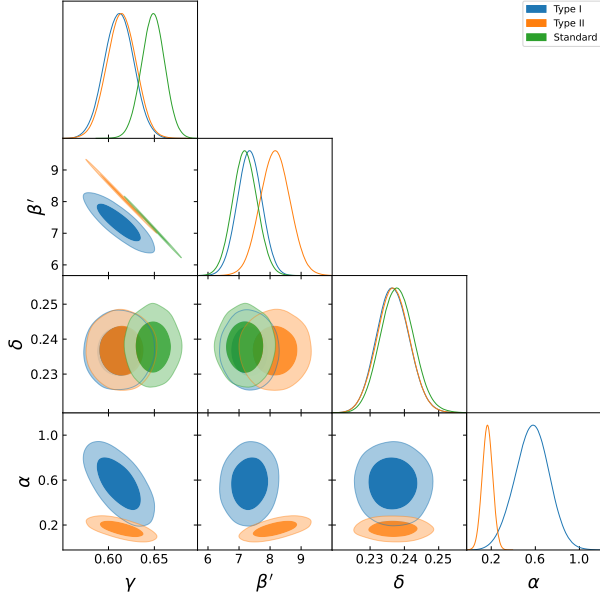


**Figure 2.** One-dimensional probability density distributions and two-dimensional contours of  $\alpha$ ,  $\beta'$ ,  $\gamma$ , and  $\delta$  from the low-redshift quasars. The blue, orange, and green contours represent the Type I, Type II, and standard relations, respectively.

tion in relation to cosmology<sup>4</sup>. Here we set a fiducial model: the flat  $\Lambda$ CDM model with  $H_0 = 73.04 \text{ km s}^{-1}\text{Mpc}^{-1}$  and  $\Omega_{m0} = 0.33$  for calculating the luminosity of quasars, and choose the flux limit  $F_{\text{lim}} = 6 \times 10^{-33} \text{ erg s}^{-1}\text{cm}^{-2}\text{Hz}^{-1}$  for the X-rays and  $F_{\text{lim}} = 4.5 \times 10^{-29} \text{ erg s}^{-1}\text{cm}^{-2}\text{Hz}^{-1}$  for the UV. We finally obtain  $k_X = 7.10 \pm 0.17$  and  $k_{UV} = 9.76 \pm 0.22$  for the Type I relation, and  $k_X = 2.64 \pm 0.06$  and  $k_{UV} = 3.62 \pm 0.08$  for the Type II relation. Using the fiducial model to estimate the luminosity distance, the value of parameter  $\gamma$  can then be determined from Eq. (8) with the whole quasar sample, and the results are  $\gamma = 0.579 \pm 0.011$  and  $\gamma = 0.577 \pm 0.011$  for the Type I and II relations, respectively. Finally, we use Eq. (9) to calculate the mean value of  $\alpha$  with  $1\sigma$  uncertainty, and obtain  $\alpha = 0.629 \pm 0.103$  and  $\alpha = 0.239 \pm 0.037$ <sup>5</sup> for the Type I and II relations, respectively. These results deviate from zero at more than  $5\sigma$  and are compatible with those obtained from the low-redshift calibration and shown in Tab. 1 within  $2\sigma$  CL. This compatibility suggests that the nonzero value of  $\alpha$  from the low-redshift calibration is unlikely to result from selection biases or redshift evolution in quasars. It is worth noting that the bias due to extinction on quasar luminosity distances has been studied recently in (Zajack et al. 2024).

### 3 CONSTRAINTS ON COSMOLOGICAL MODELS

Extrapolating the values of  $\alpha$ ,  $\beta'$ ,  $\gamma$  and  $\delta$  from the low-redshift data to the high-redshift regions, we can obtain the luminosity distance of all quasar data. These data can now be employed to constrain the cosmological models by finding the maximum likelihood of the

<sup>4</sup> <https://notebookarchive.org/2023-05-8b2lbrh>

<sup>5</sup> This result is different from  $0.342 \pm 0.041$  obtained in (Dainotti et al. 2022b) since the luminosity is corrected as  $L' = L/g(z)$  with  $g(z) = z^k z_{\text{crit}}^k / (z^k + z_{\text{crit}}^k)$  rather than  $g(z) = (1+z)^k$  in (Dainotti et al. 2022b).

following function:

$$\tilde{\mathcal{L}}(\mathbf{p}) = \prod_{i=1}^N \frac{1}{\sqrt{2\pi(\tilde{\sigma}_i^2 + \delta^2)}} \times \exp \left\{ -\frac{[\log(F_X)_{\text{obs},i} - \log(F_X)_{\text{th}}(d_L(z_i, \mathbf{p}))]^2}{2(\tilde{\sigma}_i^2 + \delta^2)} \right\}. \quad (10)$$

Here  $N$  denotes the number of data, and  $\tilde{\sigma}_i$  is the derived uncertainty of  $\log(F_X)$  by using the error propagation formula

$$\begin{aligned} \tilde{\sigma}_i^2 &= \sigma_{\log(F_X)_{\text{obs},i}}^2 + \left( \frac{\partial \log(F_X)_{\text{th}}}{\partial \gamma} \right)_i^2 \sigma_\gamma^2 \\ &+ \left( \frac{\partial \log(F_X)_{\text{th}}}{\partial \beta'} \right)_i^2 \sigma_{\beta'}^2 + \left( \frac{\partial \log(F_X)_{\text{th}}}{\partial \alpha} \right)_i^2 \sigma_\alpha^2 \\ &+ \left( \frac{\partial \log(F_X)_{\text{th}}}{\partial \log(F_{UV})_{\text{obs}}} \right)_i^2 \sigma_{\log(F_{UV})_{\text{obs}}}^2 \\ &+ 2 \sum_{j=1}^3 \sum_{k=j+1}^3 \left( \frac{\partial \log(F_X)_{\text{th}}}{\partial \theta_j} \frac{\partial \log(F_X)_{\text{th}}}{\partial \theta_k} \right)_i C_{jk}, \end{aligned} \quad (11)$$

where  $C_{jk}$  is the covariance matrix, and  $\sigma_\alpha$ ,  $\sigma_{\beta'}$ , and  $\sigma_\gamma$  are the uncertainties of coefficients  $\alpha$ ,  $\beta'$ , and  $\gamma$  estimated from the GP, respectively. In Eq. (10),  $\mathbf{p}$  represents the cosmological model parameters and  $m$  is the apparent magnitude derived from the cosmological model, which relates to the dimensionless luminosity distance  $D_L$  through

$$m(z, \mathbf{p}) = 5 \log D_L(z; \mathbf{p}) + M, \quad (12)$$

with

$$M = 25 + M - 5 \log \frac{c}{H_0}. \quad (13)$$

The dimensionless luminosity distance is defined as

$$D_L(z; \mathbf{p}) = \frac{H_0}{c} d_L(z; \mathbf{p}) = (1+z) \int_0^z \frac{d\tilde{z}}{E(\tilde{z}; \mathbf{p})} \quad (14)$$

in the spatially flat universe. Here,  $E(z; \mathbf{p})$  is the dimensionless Hubble parameter. For the  $w$ CDM model,  $E(z; \mathbf{p})$  has the form

$$E(z; \mathbf{p})^2 = \Omega_{m0}(1+z)^3 + (1 - \Omega_{m0})(1+z)^{3(1+w)}, \quad (15)$$

where  $\Omega_{m0}$  and  $w$  are the current matter density and the equation of state (EOS) of dark energy, respectively. This model will reduce to the  $\Lambda$ CDM when  $w = -1$ . Therefore, we have  $\mathbf{p} \equiv \{\Omega_{m0}\}$  for the  $\Lambda$ CDM model and  $\mathbf{p} \equiv \{w, \Omega_{m0}\}$  for the  $w$ CDM model. Here the prior of  $w$  is set as a uniform distribution in  $1/(\Omega_{m0} - 1) \leq w \leq -1/3$ , which comes from the accelerated cosmic expansion (Riess et al. 1998; Perlmutter et al. 1999) and the null energy condition (Visser & Barcelo 2000; Lenart et al. 2023). Since  $M$  and  $H_0$  can not be constrained simultaneously when only quasars are used,  $M$  is treated as a nuisance parameter, and is marginalized in our analysis.

#### 3.1 Constraints on cosmological models from Quasars

In Sec. II, we have used the SN Ia data in the redshift region of  $z \leq 1.4$  to calibrate the quasars in this redshift region and extrapolate the results to the high-redshift ( $z > 1.4$ ) quasars. Thus, the high-redshift quasars, which contain 1095 observations, are utilized firstly to constrain the  $\Lambda$ CDM and  $w$ CDM models. Furthermore, we also consider the full-redshift quasar data (2421 data points) to limit these two models. The results are shown in Figs. 3 and 4, and summarized in Tab. 3.

It is easy to see that for the  $\Lambda$ CDM model when the standard  $L_X$ - $L_{UV}$  relation is used, quasars only give a lower bound on  $\Omega_{m0}$ . The

**Table 1.** Marginalized one-dimensional constraints on parameters with  $1\sigma$  CL from the low-redshift ( $z \leq 1.4$ ) quasars

Relations	$\delta$	$\alpha$	$\beta'$	$\gamma$	$-2 \ln \mathcal{L}$
standard	$0.2379 \pm 0.0049$	-	$7.19 \pm 0.40$	$0.649 \pm 0.013$	0.939
Type I	$0.2360^{+0.0046}_{-0.0051}$	$0.57 \pm 0.15$	$7.33 \pm 0.41$	$0.612 \pm 0.016$	-12.270
Type II	$0.2370 \pm 0.0049$	$0.165 \pm 0.046$	$8.19 \pm 0.48$	$0.613 \pm 0.016$	-11.562

**Table 2.** Marginalized one-dimensional constraints on parameters with  $1\sigma$  CL from the quasars in two different redshift regions

Redshift regions	Relations	$\delta$	$\alpha$	$\beta'$	$\gamma$
$0 < z \leq 1.0$	Standard	$0.2352 \pm 0.0059$	-	$7.45 \pm 0.54$	$0.640 \pm 0.018$
	Type I	$0.2350 \pm 0.0061$	$0.42^{+0.18}_{-0.24}$	$7.18 \pm 0.56$	$0.625 \pm 0.020$
	Type II	$0.2350 \pm 0.0060$	$0.111^{+0.048}_{-0.069}$	$7.81 \pm 0.59$	$0.626 \pm 0.019$
$0 < z \leq 1.8$	Standard	$0.2358 \pm 0.0042$	-	$7.16 \pm 0.32$	$0.650 \pm 0.010$
	Type I	$0.2339 \pm 0.0042$	$0.51 \pm 0.11$	$7.59 \pm 0.33$	$0.607 \pm 0.013$
	Type II	$0.2341 \pm 0.0042$	$0.165 \pm 0.036$	$8.39 \pm 0.42$	$0.607 \pm 0.014$

full-redshift quasars with Type II relation give an effective constraint on  $\Omega_{m0}$ , while the high-redshift ones do not. When Type I relation is used, both the full- and high-redshift quasars can constrain  $\Omega_{m0}$  effectively. For the  $w$ CDM model, the effective constraints on  $\Omega_{m0}$  and  $w$  can be achieved only from the full-redshift quasars with Type I or II relation. In both the  $\Lambda$ CDM and  $w$ CDM models, quasars with Type I relation always tend to give smaller  $\Omega_{m0}$  and  $-2 \ln \mathcal{L}$  than those with the standard and Type II relations.

Since the cosmological parameters  $\Omega_{m0}$  and  $w$  cannot be well constrained simultaneously, we further consider a fitting for  $w$  with  $\Omega_{m0}$  fixed to be 0.30. The results are shown in Fig. 5. Apparently, for all three relations the high-redshift quasars only give the lower limit of  $w$ . When the full-redshift quasars are used, we obtain that  $w = -1.08^{+0.17}_{-0.34}$  for Type I relation and  $w = -1.02^{+0.63}_{-0.41}$  for Type II relation. If the standard relation is considered, a large  $w$  ( $-0.381 < w < -1/3$ ) is obtained.

### 3.2 Constraints on cosmological models from Quasars + OHD

Since quasars cannot provide the constraints on  $M$  and  $H_0$  due to the degeneracy between them, we further add the OHD from the cosmic age difference method (Jimenez & Loeb 2002) into our analysis. The updated 32 OHD measurements cover a redshift range of  $0.07 < z < 1.965$  (Moresco et al. 2020), which contains 17 uncorrelated and 15 correlated measurements. The 17 uncorrelated data are given in (Zhang et al. 2014; Simon, Verde & Jimenez 2005; Ratsimbazafy et al. 2017) and the 15 correlated measurements are sourced from (Moresco et al. 2012; Moresco 2015; Moresco et al. 2016) with the covariance matrix being given by Moresco et al. (2020). To constrain the cosmological models, the minimization of the  $\chi^2$  method is used:

$$\chi_{\text{OHD}}^2(\mathbf{p}) = \sum_{i=1}^{17} \frac{[H_{\text{th}}(z_i; \mathbf{p}) - H_{\text{obs}}(z_i)]^2}{\sigma_{H,i}^2} + \Delta \hat{H}^T \mathbf{C}_H^{-1} \Delta \hat{H}. \quad (16)$$

Here  $\sigma_H$  represents the observed uncertainty of 17 uncorrelated measurements,  $\Delta \hat{H} = H_{\text{th}}(z; \mathbf{p}) - H_{\text{obs}}(z)$  represents the difference vector between the observed data and the theoretical values for the 15

correlated measurements, and  $\mathbf{C}_H^{-1}$  is the inverse of the covariance matrix.  $H_{\text{obs}}$  represents the observed value of the Hubble parameter, while  $H_{\text{th}}(z; \mathbf{p}) \equiv H_0 E(z; \mathbf{p})$  is the corresponding theoretical one calculated from the cosmological model.

The constraints on the cosmological models from quasars+OHD can be obtained from the total likelihood:

$$\ln \mathcal{L}_{\text{total}}(\mathbf{p}) = \ln \tilde{\mathcal{L}}(\mathbf{p}) - \frac{1}{2} \chi_{\text{OHD}}^2(\mathbf{p}). \quad (17)$$

The results are shown in Figs. 6 and 7, and summarized in Tab. 4.

For the  $\Lambda$ CDM model, we find that in the case of the standard  $L_X$ - $L_{UV}$  relation the combination of the full-redshift quasars and the OHD measurements favors a smaller  $H_0$ , a larger  $\Omega_{m0}$ , and a larger  $M$  than the high-redshift quasars plus OHD. The differences between the values of the cosmological model parameters and the absolute magnitude respectively from the high- and full-redshift quasars found in the standard relation become negligible when the Type II or Type I relation is used instead. In the Type II relation, the value of  $H_0$  is consistent with the result from the Planck CMB observations (Planck Collaboration 2020), while the value of  $M$  is smaller than the SH0ES measurement (Riess et al. 2022). When the Type I relation is considered, we find that the  $H_0$  value from full-redshift quasars locates between the Planck result and the SH0ES measurement (Riess et al. 2022; Planck Collaboration 2020), and the  $M$  value is compatible with the SH0ES measurement (Riess et al. 2022).

For the  $w$ CDM model, we find that there is a large difference between the constraints on  $H_0$  obtained from the high- and full-redshift quasars in the standard  $L_X$ - $L_{UV}$  relation, and this difference reduces to be very small when the Type I or II relation is considered. For the standard relation, the full-redshift quasars favor a smaller  $H_0$  than the high-redshift data, but the results obtained in the Type I and II relations are opposite. For Type I and II relations, the constraints on  $\Omega_{m0}$  obtained from the high- and full-redshift quasars are very close, while the values obtained from Type I relation are always smaller than those obtained from Type II one. The standard relation gives two significantly different  $\Omega_{m0}$  from the full- and high-redshift quasars, respectively, which are larger than those obtained in Type I and II relations. In the three relations, quasars can always give

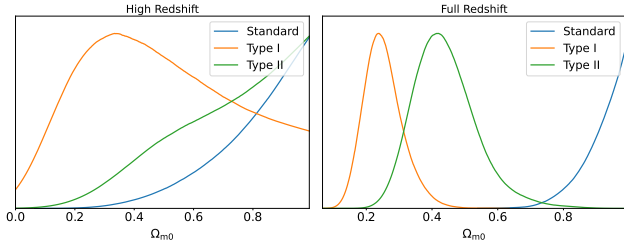


**Figure 3.** The marginalized probability density distributions of  $\Omega_{m0}$  in the  $\Lambda$ CDM model, obtained from high-redshift ( $z > 1.4$ ) and full-redshift quasars, are analyzed for three different  $L_X$ - $L_{UV}$  relations.

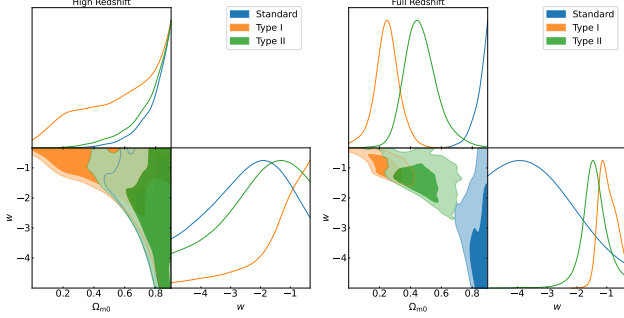


**Figure 4.** Constraints on  $\Omega_{m0}$  and  $w$  in the  $w$ CDM model, obtained from high-redshift ( $z > 1.4$ ) and full-redshift quasars, are analyzed for three different  $L_X$ - $L_{UV}$  relations.

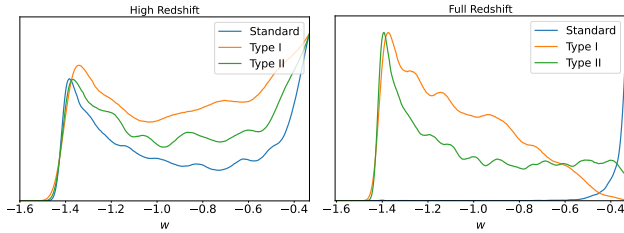


**Figure 5.** Constraints on  $w$  with  $\Omega_{m0} = 0.30$  in the  $w$ CDM model from high-redshift ( $z > 1.4$ ) and full-redshift quasars.

constraints on  $w$  consistent with  $-1$  at  $2\sigma$  CL. The constraints on  $M$  obtained from both the high- and full-redshift quasars in these three relations are nearly identical to that obtained in the  $\Lambda$ CDM model. Furthermore, quasars with the Type I relation have the minimum value of  $-2 \ln \mathcal{L}$ .

#### 4 DISCUSSION

Except for the low-redshift calibration, the global fitting method is usually used to avoid the so-called circularity problem. Using the total 2421 quasar datapoints to constrain the spatially flat  $\Lambda$ CDM model and the coefficients in the  $L_X$ - $L_{UV}$  relations simultaneously, it has been found that  $\Omega_{m0} > 0.924$ ,  $\delta = 0.228 \pm 0.004$ ,  $\beta = 7.021 \pm 0.249$  and  $\gamma = 0.639 \pm 0.008$  for the standard relation, and  $\Omega_{m0} = 0.510^{+0.163}_{-0.254}$ ,  $\delta = 0.225 \pm 0.004$ ,  $\beta = 7.825 \pm 0.316$ ,  $\gamma = 0.579 \pm 0.011$  and  $\alpha = 0.580^{+0.084}_{-0.099}$  for Type I relation (Wang et al. 2022). Apparently, the values of relation coefficients and intrinsic dispersion from the global fitting are well consistent with those shown Tab. 1, and the values of  $\Omega_{m0}$  are compatible with those (see Tab. 3) from

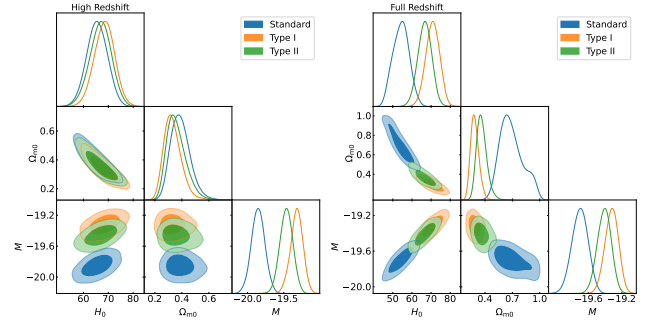


**Figure 6.** Constraints on  $H_0$ ,  $\Omega_{m0}$  and  $M$  in the  $\Lambda$ CDM model for three different  $L_X$ - $L_{UV}$  relations, obtained from high-redshift ( $z > 1.4$ ) and full-redshift quasars plus OHD.

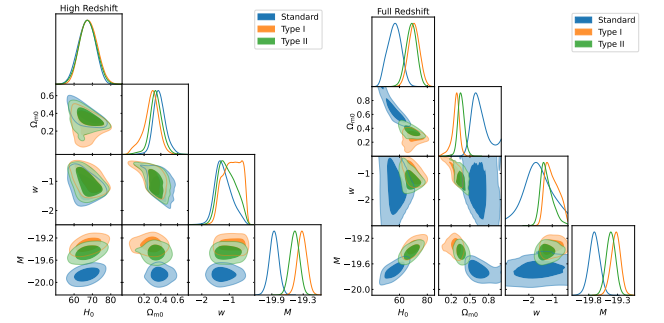


**Figure 7.** Constraints on  $H_0$ ,  $\Omega_{m0}$ ,  $w$  and  $M$  in the  $w$ CDM model for three different  $L_X$ - $L_{UV}$  relations, obtained from high-redshift ( $z > 1.4$ ) and full-redshift quasars plus OHD.

the high-redshift quasars. In the flat  $\Lambda$ CDM model, quasars in the redshift region  $0.0041 \leq z \leq 1.686$  give that the best fitting values are  $\Omega_{m0} = 0.995$ ,  $\delta = 0.329$  and  $\gamma = 0.559$  (Khadka et al. 2023). These values of  $\delta$  and  $\gamma$  are compatible with those shown in Tab. 1. Assuming a cosmological model with parameter values based on the computations with SNe Ia, Lenart et al. (2023) obtained that  $\delta = 0.231 \pm 0.004$ ,  $\beta = 6.817 \pm 0.265$ ,  $\gamma = 0.648 \pm 0.009$  for the standard relation, and  $\delta = 0.231 \pm 0.004$ ,  $\beta = 8.278 \pm 0.362$ ,  $\gamma = 0.591 \pm 0.013$  for the Type II relation with  $\alpha$  fixed from the EP method. These results are also consistent with ours obtained from the low redshift calibration. Comparing Fig. 2 with Fig. 2a and 2b in (Dainotti et al. 2023c) and Figs. 2 and 3 in (Bargiacchi et al. 2023), we find that the values of intrinsic dispersion and coefficients of the standard and Type II relations obtained in this paper are compatible with what were determined from the combination of Pantheon SN Ia, GRBs, quasars and BAO in the  $\Lambda$ CDM model. While, the values of  $H_0$  in the standard and Type II relations are slightly smaller than what were obtained in (Dainotti et al. 2023c). The values of  $\delta$  achieved in (Dainotti et al. 2023c; Lenart et al. 2023; Wang et al. 2022) and this paper are significant larger than  $\delta = 0.007 \pm 0.004$  from the golden sample of 983 quasars (Dainotti et al. 2023a). Interestingly, the constraint on  $\Omega_{m0}$  from quasars with Type I relation is well consistent with  $\Omega_{m0} = 0.240 \pm 0.064$  from 1253 gold quasar sample (Dainotti et al. 2024) and  $\Omega_{m0} = 0.295^{+0.013}_{-0.012}$  from SN Ia + quasars (Bargiacchi et al. 2022). Recently, Bargiacchi, Dainotti & Capozziello (2023) found that the high-redshift evolution of our universe from GRBs and quasars in the case of Type II relation with the effect of redshift evolution being fixed by using the EP method has a strong tension with the prediction of the  $\Lambda$ CDM model. Whether this tension still

**Table 3.** Constraints on the  $\Lambda$ CDM and  $w$ CDM models from Quasars.

Relation	Model	Data Set	$\Omega_{m0}$	$w$	$-2 \ln \mathcal{L}$
Standard	$\Lambda$ CDM	$z > 1.4$	$> 0.765$	-	-94.716
		full $z$	$> 0.903$	-	-95.963
Type I	$\Lambda$ CDM	$z > 1.4$	$0.49^{+0.21}_{-0.33}$	-	-129.022
		full $z$	$0.253^{+0.046}_{-0.067}$	-	-153.029
Type II	$\Lambda$ CDM	$z > 1.4$	$> 0.622$	-	-129.191
		full $z$	$0.440^{+0.073}_{-0.11}$	-	-147.054
Standard	$w$ CDM	$z > 1.4$	$> 0.766$	$-3.23^{+2.8}_{-0.70}$	-94.156
		full $z$	$> 0.834$	$-4.4^{+2.3}_{-1.8}$	-94.305
Type I	$w$ CDM	$z > 1.4$	$> 0.468$	$> -2.08$	-129.631
		full $z$	$0.249 \pm 0.082$	$-0.98^{+0.25}_{-0.34}$	-153.638
Type II	$w$ CDM	$z > 1.4$	$> 0.724$	$> -3.30$	-129.057
		full $z$	$0.469^{+0.084}_{-0.12}$	$-1.43 \pm 0.45$	-149.635

Note—The marginalized mean values, the standard deviations, and the 68% CL.

**Table 4.** Constraints on the  $\Lambda$ CDM and  $w$ CDM models from quasars and OHD.

Relation	Model	Data Set	$H_0$	$\Omega_{m0}$	$w$	$M$	$-2 \ln \mathcal{L}$
Standard	$\Lambda$ CDM	$z > 1.4$	$65.5 \pm 4.2$	$0.390^{+0.059}_{-0.081}$	-	$-19.854 \pm 0.093$	-72.484
		full $z$	$54.3 \pm 4.2$	$0.693^{+0.088}_{-0.16}$	-	$-19.700 \pm 0.096$	-56.918
Type I	$\Lambda$ CDM	$z > 1.4$	$68.5 \pm 4.1$	$0.332^{+0.050}_{-0.073}$	-	$-19.321^{+0.090}_{-0.079}$	-114.503
		full $z$	$70.8 \pm 3.6$	$0.289^{+0.038}_{-0.051}$	-	$-19.321^{+0.085}_{-0.076}$	-137.804
Type II	$\Lambda$ CDM	$z > 1.4$	$66.9 \pm 4.3$	$0.361^{+0.052}_{-0.083}$	-	$-19.464 \pm 0.090$	-111.631
		full $z$	$66.7 \pm 3.6$	$0.364^{+0.045}_{-0.063}$	-	$-19.410 \pm 0.083$	-131.713
Standard	$w$ CDM	$z > 1.4$	$66.9 \pm 4.6$	$0.384^{+0.061}_{-0.078}$	$-1.22^{+0.24}_{-0.35}$	$-19.858 \pm 0.089$	-73.892
		full $z$	$56.0^{+5.5}_{-4.8}$	$0.658^{+0.076}_{-0.16}$	$-1.69^{+0.67}_{-0.75}$	$-19.702 \pm 0.092$	-58.194
Type I	$w$ CDM	$z > 1.4$	$67.9^{+4.4}_{-5.0}$	$0.283^{+0.10}_{-0.070}$	$-0.89^{+0.45}_{-0.25}$	$-19.320 \pm 0.089$	-114.503
		full $z$	$70.5 \pm 4.0$	$0.272^{+0.067}_{-0.040}$	$-1.01^{+0.22}_{-0.37}$	$-19.330 \pm 0.083$	-138.321
Type II	$w$ CDM	$z > 1.4$	$67.5 \pm 4.6$	$0.342 \pm 0.079$	$-1.07^{+0.27}_{-0.39}$	$-19.465 \pm 0.091$	-112.232
		full $z$	$68.5 \pm 3.9$	$0.360^{+0.048}_{-0.054}$	$-1.24^{+0.18}_{-0.31}$	$-19.416 \pm 0.081$	-133.843

Note—The marginalized mean values, the standard deviations, and the 68% CL.

exists for quasars with Type I relation is an interesting topic and needs to be investigated in the future.

## 5 CONCLUSIONS

In this paper, we compare the constraints on the cosmological models from quasars with three different  $L_X$ - $L_{UV}$  relations: the standard relation proposed by Risaliti & Lusso (2015), and the Type I and Type II redshift-evolutionary relations constructed by Wang et al. (2022) and Dainotti et al. (2022b), respectively. We employ the GP method to calibrate these relations from the latest Pantheon+ SN Ia data within the low-redshift region ( $z < 1.4$ ). These results align with that reported by Wang et al. (2022), and suggest a potential trend of redshift evolution in the  $L_X$ - $L_{UV}$  relation.

Extrapolating the calibrated relations from the low-redshift quasars to the quasars that lie in high-redshift region, we obtain the luminosity distances of quasars and then constraints from them on the spatially flat  $\Lambda$ CDM and  $w$ CDM models. We find that the standard relation provides only a lower bound on  $\Omega_{m0}$  in both the  $\Lambda$ CDM and  $w$ CDM

models. For the  $\Lambda$ CDM model, Type II relation gives effective constraints on the cosmological model parameters only when the full-redshift quasars are used. In contrast, Type I relation always can offer tight constraints on the cosmological model parameters, since the mean values of  $\Omega_{m0}$  with  $1\sigma$  CL are  $\Omega_{m0} = 0.49^{+0.21}_{-0.33}$  for the high-redshift quasars and  $\Omega_{m0} = 0.253^{+0.046}_{-0.067}$  for the full-redshift data. For the  $w$ CDM model, Type I relation yields the  $\Omega_{m0} = 0.249 \pm 0.082$  and  $w = -0.98^{+0.25}_{-0.34}$  when the full-redshift data is used, which are consistent with those obtained from the CMB data (Planck Collaboration 2020). Additionally, Type I relation always tends to give smaller values of  $-2 \ln \mathcal{L}$  than those of the standard and Type II relations in both the  $\Lambda$ CDM and  $w$ CDM models.

When the additional OHD sample is considered, the observations can give tight constraints on the  $\Lambda$ CDM and  $w$ CDM models in all three relations, while the  $\Lambda$ CDM model constrained from quasars with the Type I relation still yields the tightest results. For this preferred model, we find that the constraints on  $\Omega_{m0}$  are  $0.332^{+0.050}_{-0.073}$  for the high-redshift quasars and  $0.289^{+0.038}_{-0.051}$  for the full-redshift quasars, which are consistent with the CMB results (Planck Collab-

oration 2020). Moreover, since the addition of the OHD sample can break the degeneracy between parameters  $M$  and  $H_0$ , we obtain the following constraints on them. In the  $\Lambda$ CDM model, the OHD measurements plus the full-redshift quasars with the Type I relation give the absolute magnitude  $M$  to be  $-19.321^{+0.085}_{-0.076}$ , which aligns well with that obtained from SH0ES ( $M = -19.253 \pm 0.027$ ) (Riess et al. 2022), and the Hubble constant  $H_0$  to be  $70.80 \pm 3.6 \text{ km s}^{-1} \text{ Mpc}^{-1}$ , which lies between the measurements of SH0ES (Riess et al. 2022) and CMB (Planck Collaboration 2020).

## ACKNOWLEDGMENTS

This project was supported by the NSFC under Grants Nos. 12275080 and 12075084, the innovative research group of Hunan Province under Grant No. 2024JJ1006, and the Guizhou Provincial Science and Technology Foundation (QKHJC-ZK[2021] Key 020).

## DATA AVAILABILITY

Data are available at the following references: the 2421 X-ray and UV flux measurements of quasars from Lusso et al. (2020), the Pantheon+ SNe Ia sample from Scolnic et al. (2022), and the latest OHD obtained with the cosmic chronometer method from Moresco et al. (2020).

## REFERENCES

- Alam, S., et al. [eBOSS Collaboration], 2021, *Phys. Rev. D*, 103, 083533
- Avni, Y., & Tananbaum, H. 1986, *ApJ*, 305, 83
- Bañados, E., Venemans, B., Mazzucchelli, C., et al. 2017, *Nature*, 553, 473
- Bargiacchi, G., Benetti, M., Capozziello, S., et al. 2022, *MNRAS*, 515, 1795
- Bargiacchi, G., Dainotti, M., Nagataki, S., Capozziello, S. 2023, *MNRAS*, 521, 3909
- Bargiacchi, G., Dainotti, M., & Capozziello, S. 2023, *MNRAS*, 525, 3104
- Bloom, J. S., Frail, D. A., & Sari, R. 2001, *AJ*, 121, 2879
- Brout, D., Scolnic, D., Popovic, B., et al. 2022, *ApJ*, 938, 110
- Busti, V. C., Clarkson, C., & Seikel, M. 2014, *MNRAS Lett.*, 441, L11
- Cao, S. & Ratra, B. *arXiv: 2404.08697*
- Capozziello, S., & Izzo, L. 2008, *A&A*, 490, 31
- D'Agostini, G. 2005, *arXiv: physics/0511182*
- Di Valentino, E., Mena, O., Pan, S., et al. 2021, *CQG*, 38, 153001
- Dainotti, M., Petrosian, V., Willingale, R., et al. 2015, *MNRAS*, 451, 3898
- Dainotti, M. G., Simone, B. D., Schiavone, T., et al. 2021, *ApJ*, 912, 150
- Dainotti, M. G., Simone, B. D., Schiavone, T., et al. 2022a, *Galaxies*, 10, 24
- Dainotti, M. G., Bargiacchi, G., Lenart, A. L., et al. 2022b, *ApJ*, 931, 106
- Dainotti, M. G., Bargiacchi, G., Lenart, A. L., et al. 2023a, *ApJ*, 950, 45
- Dainotti, M. G., Lenart, A. L., Chraya, A., et al. 2023b, *MNRAS*, 518, 2201
- Dainotti, M. G., Bargiacchi, G., Bogdan, M., et al. 2023c, *ApJ*, 951, 63
- Dainotti, M. G., Lenart, A. L., Yengejeh, M., et al. 2024, *Phys. of Dark Univ.*, 44, 101428
- Demianski, M., Piedipalumbo, E., Sawant, D., & Amati, L. 2017, *A&A*, 598, A112
- Efron, B., & Petrosian, V. 1992, *ApJ*, 399, 345
- Eisenstein, D. J., Zehavi, I., Hogg, D. W., et al. 2005, *ApJ*, 633, 560
- Foreman-Mackey, D., Hogg, D. W., Lang, D., & Goodman, J. 2013, *PASP*, 125, 306
- Ghirlanda, G., Ghisellini, G., Lazzati, D., & Firmani, C. 2004, *ApJ*, 613, L13
- Hu, J. P., & Wang, F. Y. 2022a, *A&A*, 661, A71
- Hu, J. P., & Wang, F. Y. 2022b, *MNRAS*, 517, 576
- Jimenez, R., & Loeb, A. 2002, *ApJ*, 573, 37
- Kodama, Y., Yonetoku, D., Murakami, T., et al. 2008, *MNRAS Lett.*, 391, L1
- Khadka, N. & Ratra, B. 2021, *MNRAS*, 502, 6140
- Khadka, N. & Ratra, B. 2020a, *MNRAS*, 492, 4456
- Khadka, N. & Ratra, B. 2020b, *MNRAS*, 497, 263
- Khadka, N. et al. 2023, *MNRAS*, 522, 1247
- Lenart, A. L., Bargiacchi, G., Dainotti, M. G., Nagataki, S., & Capozziello, S. 2023, *ApJS*, 264, 46
- Li, H., Xia, J.-Q., Liu, J., et al. 2008, *ApJ*, 680, 92
- Lin, H.-N., Li, M.-H., & Li, X. 2018, *MNRAS*, 480, 3117
- Li, X., Keeley, R. E., Shafieloo, A., et al. 2021, *MNRAS*, 507 919
- Li, X., Keeley, R. E., Shafieloo, A., & Liao, K. 2024, *ApJ*, 960, 103
- Liang, N., Xiao, W. K., Liu, Y., & Zhang, S. N. 2008, *ApJ*, 685, 354
- Liang, N., Wu, P., & Zhang, S. N. 2010, *Phys. Rev. D*, 81, 083518
- Liang, N., Xu, L., & Zhu, Z. H. 2011, *A&A*, 527, A11
- Liang, N., Li, Z., Xie, X., & Wu, P. 2022, *ApJ*, 941, 84
- Liu, J., & Wei, H. 2015, *GRGr*, 47, 141
- Liu, Y., Chen, F., Liang, N., et al. 2022, *ApJ*, 931, 50
- Liu, Y., Liang, N., Xie, X., et al. 2022, *ApJ*, 935, 7
- Liu, Y., Yu, H., & Wu, P. 2023, *ApJ*, 946, L49
- Lusso, E. & Risaliti, G. 2016, *ApJ*, 819, 154
- Lusso, E. & Risaliti, G. 2017, *A&A*, 602, A79
- Lusso, E., Piedipalumbo, E., Risaliti, G., et al. 2019, *A&A*, 628, L4
- Lusso, E., Risaliti, G., Nardini, E., et al. 2020, *A&A*, 642, A150
- Mortlock, D., Warren, S., Venemans, B., et al. 2011, *Nature*, 474, 616
- Moresco, M., Cimatti, A., Jimenez, R., et al. 2012, *J. Cosmology Astropart. Phys.*, 08, 006
- Moresco, M. 2015, *MNRAS*, 450, L16
- Moresco, M., Pozzetti, L., Cimatti, A., et al. 2016, *J. Cosmology Astropart. Phys.*, 05, 014
- Moresco, M., Jimenez, R., Verde, L., et al. 2020, *ApJ*, 898, 82
- Mu, Y., Chang, B., & Xu, L., 2023, *CQG*, 40, 225003
- Nelsen, R. B. 2007, *An Introduction to Copulas* (New York: Springer). 2023, *J. Cosmology Astropart. Phys.*, 09, 041
- Pan, Y., Qi, J., Cao, S., et al. 2020, *ApJ*, 890, 169
- Perivolaropoulos, L., & Skara, F., 2022, *New Astron. Rev.*, 95, 101659
- Perlmutter, S., Aldering, G., Goldhaber, G., et al. 1999, *ApJ*, 517, 565
- Planck Collaboration 2020, *A&A*, 641, 67
- Ratsimbazafy, A. L., Loubser, S. I., Crawford S. M., et al. 2017, *MNRAS*, 467, 3239
- Riess A. G. 2020, *Nature Rev. Phys.*, 2, 10
- Riess, A. G., Filippenko, A. V., Challis, P., et al. 1998, *AJ*, 116, 1009
- Riess, A. G., Yuan, W., Macri, L. M., et al. 2022, *ApJ*, 934, L7
- Risaliti, G. & Lusso, E. 2015, *ApJ*, 815, 33
- Risaliti, G. & Lusso, E. 2019, *NatAs*, 3, 272
- Simon, J., Verde L., & Jimenez R., 2005, *Phys. Rev. D*, 71, 123001
- Singal, J., Mutchnick, S., & Petrosian, V. 2022, *ApJ*, 932, 111
- Singal, J., Petrosian, V., Haider, J., & Malik, S. 2019, *ApJ*, 877, 63
- Singal, J., Petrosian, V., Stawarz, L., & Lawrence, A. 2013, *ApJ*, 764, 43
- Seikel, M., Clarkson, C., & Smith, M. 2012a, *J. Cosmology Astropart. Phys.*, 06, 036
- Seikel, M., Yahya, S., Maartens, R., & Clarkson, C. 2012b, *Phys. Rev. D*, 86, 083001
- Scolnic, D., Brout, D., Carr, A. et al. 2022, *ApJ*, 938, 113
- Suyu, S. H., Marshall, P. J., Auger, M. W. et al. 2010, *ApJ*, 711, 201
- Suyu, S. H., Auger, M. W., Hilbert, S. et al. 2013, *ApJ*, 766, 70
- Tananbaum, H., Avni, Y., Branduardi, G., et al. 1979, *ApJL*, 234, L9
- Velten, H. & Gomes, S. 2020, *Phys. Rev. D*, 101, 043502
- Visser, M., & Barcelo, C., *Energy conditions and their cosmological implications*, 2000, 98
- Wang, J. S., Wang, F. Y., Cheng, K. S., & Dai, Z. G. 2016, *A&A*, 585, A68
- Wang, F., Yang, J., Fan, X., et al. 2021, *ApJ*, 907, L1
- Wang, B., Liu, Y., Yuan, Z., Liang, N., Yu, H., & Wu, P. 2022, *ApJ*, 940, 174
- Wang, B., Liu, Y., Yu, H. & Wu, P. 2024, *ApJ*, 962, 103
- Wei, H., & Zhang, S. N. 2009, *EPJC*, 63, 139
- Wei, H., 2010, *JCAP*, 08, 020
- Wei, J.-J., 2018, *ApJ*, 868, 29
- Wei, J.-J., & Melia, F. 2020, *ApJ*, 888, 99
- Xie, H., Nong, X., Wang, H., Zhang, B., Li, Z. & Liang, N. *arXiv:2307.16467*
- Yu, H., Wang, F. Y. 2016, *ApJ*, 828, 85
- Yu, H., Ratra, B., & Wang, F.-Y. 2018, *ApJ*, 856, 3

Zamorani, G., Henry, J. P., Maccacaro, T., et al. 1981, *ApJ*, 245, 357

Zajaček, M., Czerny, N., Khadka, N., et al. 2024, *ApJ*, 961, 229

Zhang C. et al., 2014, *RAA*, 14, 1221

This paper has been typeset from a  $\text{\TeX}/\text{\LaTeX}$  file prepared by the author.